ESTUDIO MONTE CARLO SOBRE LA CALIBRACIÓN EN ENERGÍA PARA EL EXPERIMENTO ARGON DARK MATTER

MONTE CARLO STUDIES ABOUT THE ENERGY CALIBRATION FOR THE ARGON DARK MATTER EXPERIMENT

TRABAJO FIN DE MÁSTER EN FÍSICA FUNDAMENTAL

CONVOCATORIA: JUNIO 2012

CALIFICACIÓN: 9.5

Autora:

Bárbara Montes Núñez[1]

Directores:

Luciano Romero Barajas[2]

Dpto. de Tecnología (CIEMAT)

Roberto Santorelli[3]

Dpto. de Investigación básica (CIEMAT)

[1] E-mail: barbara.montes@ciemat.es
[2] E-mail: luciano.romero@ciemat.es
[3] E-mail: roberto.santorelli@ciemat.es

Abstract

The aim of the present work is the study of the energy calibration with external radioactive sources for the Argon Dark Matter (ArDM) experiment, which consists of a double-phase argon detector for direct dark matter searches. This experiment, with a ton-scale sensitive volume, has been conceived to detect nuclear recoils produced by dark matter particles scattering off target nuclei. The advantage of having a double-phase detection technique lies on the fact that both scintillation light and ionization charge can be measured, providing a powerful discrimination method between nuclear recoils and background events. In this context, the calibration with external gamma sources is necessary in order to establish the energy scale, monitoring at the same time the detector stability. In the introduction we briefly present the different experimental evidences of dark matter and the requirements that a good particle candidate should fulfill according to the astrophysical observations. Moreover, we will introduce the supersymmetry, the extension of the Standard Model of particles which provides one WIMP candidate called neutralino. Throughout the following sections, special attention will be dedicated to the different techniques used for dark matter detection, pointing out the ArDM detector concept and technology. Finally, the simulation software and the results of the energy calibration studies will be presented.

Resumen

El propósito del presente trabajo es el estudio de la calibración en energía con fuentes radioactivas externas para el experimento Argon Dark Matter (ArDM), el cual consiste en un detector de argón de doble fase para búsqueda directa de materia oscura. Este experimento, con un volumen sensible de la escala de la tonelada, ha sido concebido para detectar retrocesos nucleares producidos en el proceso de scattering de partículas de materia oscura con núcleos blanco. La ventaja de tener una técnica de detección de doble fase reside en el hecho de que tanto la señal de centelleo como la carga de ionización pueden ser medidas, proporcionando un potente método de discriminación entre retrocesos nucleares y sucesos de fondo. En este contexto, la calibración con fuentes gamma externas es necesaria con el objeto de establecer la escala en energía al mismo tiempo que se monitoriza la estabilidad del detector. En la introducción se presentan brevemente las diferentes evidencias experimentales de materia oscura y los requisitos que un buen candidato debería satisfacer de acuerdo con las observaciones astrofísicas. Además, se introducirá la supersimetría, la extensión del Modelo Estándar de partículas que proporciona un candidato a WIMP llamado neutralino. A lo largo de las siguientes secciones, se dedicará especial atención a las diferentes técnicas empleadas para la detección de materia oscura, indicando el concepto y la tecnología del detector ArDM. Finalmente, el software de simulación y los resultados del estudio de la calibración en energía serán presentados.

Índice de contenidos

Keywords: dark matter, WIMP, direct search, nuclear recoil, noble liquid detectors, liquid argon, ArDM, energy calibration.

Palabras clave: materia oscura, WIMP, búsqueda directa, retroceso nuclear, detectores de gas noble licuado, argón líquido, ArDM, calibración en energía.

Monte Carlo studies about the energy calibration for the Argon Dark Matter experiment

Bárbara Montes Núñez
Centro de Investigaciones Energéticas, Medioambientales y Tecnológicas (CIEMAT), 28040 Madrid, Spain
(Dated: June 18, 2012)

The aim of the present work is the study of the energy calibration with external radioactive sources for the Argon Dark Matter (ArDM) experiment, which consists of a double-phase argon detector for direct dark matter searches. This experiment, with a ton-scale sensitive volume, has been conceived to detect nuclear recoils produced by dark matter particles scattering off target nuclei. The advantage of having a double-phase detection technique lies on the fact that both scintillation light and ionization charge can be measured, providing a powerful discrimination method between nuclear recoils and background events. In this context, the calibration with external gamma sources is necessary in order to establish the energy scale, monitoring at the same time the detector stability. In the introduction we briefly present the different experimental evidences of dark matter and the requirements that a good particle candidate should fulfill according to the astrophysical observations. Moreover, we will introduce the supersymmetry, the extension of the Standard Model of particles which provides one WIMP candidate called neutralino. Throughout the following sections, special attention will be dedicated to the different techniques used for dark matter detection, pointing out the ArDM detector concept and technology. Finally, the simulation software and the results of the energy calibration studies will be presented.

I. INTRODUCTION

In spite of the fact that General Relativity has been one of the most successful theories of the twentieth century, it does not give a satisfactory explanation to some cosmological and astrophysical observations. A possible description of, for example, the actual structure of the Universe at large scale and its accelerated expansion can be given by the presence of dark matter and dark energy whose nature still remains unknown.

Dark matter and dark energy components are required to account for the biggest contribution to the energy content of our Universe. According to the latest WMAP satellite data, only the 4,5% of the energy density of the Universe corresponds to barionic matter, and the non-barionic component consists of 23% dark matter, 73% dark energy and less than 1% neutrinos [1]. In the present work, we are going to focus on the nature and properties of the dark matter component.

The first possible evidence of dark matter was discovered by the Swiss astronomer Fritz Zwicky in 1933. He observed that orbital velocities of galaxies in the Coma cluster were much larger than the ones predicted theoretically by the virial theorem. In addition, this cluster would be gravitationally bound only if its total mass exceeded the mass of the luminous matter contained in its component galaxies [2]. Many other experimental evidences for dark matter have been observed during the last years, consequently, a dark matter component is required to give a satisfactory description to other observations regarding the Universe large scale structure, the gravitational lensing of background objects by galaxy clusters, such as the Bullet Cluster, and the temperature distribution of hot gas in galaxies and clusters of galaxies.

Although there are different explanations for the origin of the dark matter component, a possible description could be provided by particle physics. In this context, the dark matter component is usually assumed to be in the form of thermal relic particles produced during the Big Bang that naturally freeze-out with the right abundance and that are present now in the halo surrounding the galaxy. Considering this approach and according to the experimental results, a suitable dark matter candidate particle should fulfill the properties shown below [3]:

1. It has to be stable enough in order to be present in the actual Universe.
2. It has to be cold[1] dark matter (CDM) in order to explain the hierarchical "bottom-up" large scale structure of the Universe.
3. It should be electrically neutral and interact weakly with ordinary matter.
4. It must be massive enough to account for the measured Ω_m.

The particles satisfying the previous constraints are known as WIMPs (Weakly Interacting Massive Particles).

Supersymmetry is an extension of the Standard Model that has been developed assuming the possible existence of a natural symmetry between bosons and fermions, thus unifying matter and interactions. Supersymmetry postulates that each Standard Model particle has a superpartner (sparticle), with R parity = 1 for standard particles

[1] Particles that were not relativistic when they decoupled from radiation.

and R parity $= -1$ for supersymmetric particles, where R parity is a symmetry that forbids couplings which do not conserve baryon and lepton numbers. Our motivation for studying supersymmetry lies in the fact that it can provide a possible WIMP candidate as the lightest supersymmetric particle (LSP) called neutralino, which comes out from models with conserved R parity [4].

Considering a fourth dimensional space, bosons have integer spin while fermions have half-integer spin. The spin indicates how bosons and fermions transform under the Lorentz group. The generators of supersymmetry, Q_α, are fermionic operators and, for this reason, they transform bosons into fermions. As a result, for each bosonic state of non-zero energy, there is a fermionic state with the same energy and vice versa.

$$\begin{aligned} Q_\alpha \mid boson\rangle &= \mid fermion\rangle, \\ Q_\alpha \mid fermion\rangle &= \mid boson\rangle. \end{aligned} \tag{1}$$

The superpartners of the B and W_3 gauge bosons are called bino and wino, while the superpartners of neutral Higgs bosons H_1^0 and H_2^0 are called higgsinos. In this context, the Minimal Supersymmetric Standard Model (MSSM) contains the smallest possible field content necessary to give rise to all the fields of the Standard Model. In the MSSM, the lightest neutralino is a linear combination of the bino, wino and higgsinos [5].

$$\chi = N_{11}\tilde{B} + N_{12}\tilde{W}_3 + N_{13}\tilde{H}_1^0 + N_{14}\tilde{H}_2^0. \tag{2}$$

If R parity is conserved, sparticles must decay into an odd number of sparticles. Since LSP is the lightest sparticle, it has to be stable and can only disappear via pair annihilation, making it an excellent dark matter candidate [6].

II. DARK MATTER DETECTION

In order to determine the nature of dark matter and discriminate among the large number of candidates and models, a great experimental effort is currently undertaken. Basically, there are two different approaches to detect dark matter: direct and indirect detection. In addition, WIMPs could be also produced at high energy colliders such as the LHC [7].

The general method for indirect WIMP search is based on the detection of gamma rays or antimatter in the cosmic rays. Cosmic rays are produced in the galactic center, galactic halo or extragalactic structures such as dwarf spheroidal galaxies and clusters [8]. These particles can be measured in space-based detectors such as Fermi-LAT (gamma rays) and PAMELA or AMS (antimatter). In this regard, the observation of an excess of antiparticles or gamma rays with respect to the astrophysical background, could be an evidence of dark matter annihilations. Recently, both Fermi and PAMELA have measured the positron fraction, $e^+/(e^+ + e^-)$, obtaining an excess of positrons that increases with energy. However, this positron excess could be explained as well by astrophysical phenomena, such as pulsars emission or cosmic rays interacting with giant molecular clouds.

Indirect dark matter detection can be made by Cherenkov telescopes such as MAGIC, HESS or VERITAS or by neutrinos experiments, located underground (Super-Kamiokande), underwater (ANTARES) or underice (IceCube).

We are going to pay special attention to direct detection experiments, since ArDM belongs to this category. In such experiments, the detection of WIMPs from the galactic halo is made via elastic scattering off an ordinary target nucleus. Considering M_χ the mass of the WIMP and E_χ its energy, a nucleus of mass M_N will recoil at a scattering angle θ with an energy E_R which will be given by [9]:

$$E_R = E_\chi \frac{4M_N M_\chi}{(M_N + M_\chi)^2} \frac{(1 - cos\theta)}{2}. \tag{3}$$

If we then fold the Maxwellian kinetic energy distribution of the halo WIMPs with the above recoil distribution we get an exponentially smoothly decreasing recoil spectrum of the following form [10]

$$\frac{\mathrm{d}R}{\mathrm{d}E_R} = \frac{R_0}{< E_R >} \exp\left(-\frac{E_R}{< E_R >}\right), \tag{4}$$

where R is the interaction rate per mass unit, R_0 is the total event rate and $< E_R >$ is the average recoil energy. In our case

$$< E_R >= E_0 r, \tag{5}$$

where E_0 is the most probable incident kinetic energy of a dark matter particle and $r = \frac{4M_N M_\chi}{(M_N + M_\chi)^2}$ is a kinematic factor.

For the parameters of our galactic halo we expect recoil energies of the order of few keV to 100 keV. For this reason, detectors with keV thresholds are required. Those low energetic recoil nuclei are extremely difficult to detect and discriminate against backgrounds, thus making the WIMP direct search very challenging. Additionally, the electro-weak cross sections of neutralino interactions require large detector masses and long measuring times.

The rotation curve of the Milky Way indicates that the halo particle density should fall off with distance from the galactic center with $1/r^2$ and the mass-energy density in the vicinity of the Solar System should be around $0.3\,\mathrm{GeV/cm^3}$. Furthermore, the relative velocity of the

Solar System with respect to the halo ($\approx 244\text{kms}^{-1}$) has to be added to the Maxwellian distribution of the halo WIMPs with a dispersion of $v \approx 230\text{kms}^{-1}$. Considering these standard halo parameters, the rate depends on the WIMP mass, cross section and its average density and velocity. Detectors that are able to record at least one event per ton per day are needed if we want to reach the predicted SUSY cross sections for spin dependent and independent interactions. In argon an estimated value for the WIMP-nucleon cross section of $\sim 10^{-44}\text{cm}^2 = 10^{-8}\text{pb}$ and a WIMP mass of 100 GeV produces expected signal rates of the order of one event per ton per month [17] with 30 keV detector threshold.

Differently from the past, the new generation of dark matter experiments detect at least two signals at the same time (like ionization and scintillation or ionization and phonon) in order to carry out background discrimination.

Among the main target materials that are currently being used in the experiments we should stress: NaI (LIBRA/DAMA), Crystals (CDMS, EDELWEISS, CRESST, ROSEBUD), Liquid noble gas (WARP, XENON, XMASS, ArDM), Bubble Chamber (PICASSO), Gas detector (DRIFT) [11].

Some possible positive dark matter signals have been suggested during the past years. The DAMA [12] claim of detecting the annual modulation of the signal, due to the Earth motion around the Sun, has been widely criticized since these results are incompatible with results from other experiments, at least in the standard framework of the MSSM. The tension in the field increased after the confirmation of the result by the DAMA/LIBRA [13] experiment on several years and high statistical significance.

More recently other claims that came from CoGeNT [14] and CRESST [15] triggered additional interest on the space corresponding to so-called low-mass candidates with a WIMP mass of the order of 10 GeV.

Among all the direct detection experimental techniques, liquid noble gases, such as Argon and Xenon, have special properties providing several advantages for detecting nuclear recoils, such as:

1. They provide an appropriate target for ton-scale experiments because of their density thus allowing to build large detectors exploring low cross section values.
2. The ionization signal can be used to provide the event position reconstruction in a Time Projection Chamber (TPC), which allows the possibility of fiducial volume cuts.
3. They have good scintillation properties, being transparent to their own scintillation light. The maximum possible scintillation yield in liquid argon is about 51 photons per keV of deposited energy [16].
4. They can provide two different methods for discrimination between electron-like recoils and nuclear recoils such as differences in pulse shape and in charge to light ratio.
5. Noble gases do not attach electrons and they can be easily purified, which implies a high electron mobility and long drift distances ($D > 1m$).
6. They are safe targets because they are inert, not flammable and also very good dielectrics.

While argon and xenon have similar properties, there are different reasons to choose liquid argon instead of xenon for the experiment. Firstly, if we take into account the form factors in the cross section, the event rate in argon is less sensitive to the threshold on the recoil energy than it is for xenon. Secondly, argon is much cheaper and available in large quantity than other noble gases and, for this reason, a ton-scale detector with liquid argon is the most affordable and competitive option. In addition, there is some experience in handling massive liquid argon detectors provided by the ICARUS project. Finally, xenon and argon recoil spectra are different due to kinematics, which provides an important cross check in the case of a positive signal [17].

III. THE ARGON DARK MATTER EXPERIMENT

The aim of the Argon Dark Matter (ArDM) experiment, which consists of a ton-scale double-phase liquid argon (LAr) detector, is the direct detection of dark matter (WIMPs). The experimental setup consists of a cylindric dewar with $\sim 80\,\text{cm}$ diameter sensitive volume, delimited by a reflector covered with wavelength shifter, and a 120 cm maximal drift length. About $\sim 850\,\text{kg}$ of ultra-clean liquid argon are contained in the sensitive volume. The setup is completed with cryogenic and purification systems and a polyethylene shield (Figure 1). In order to test all the functionalities, the LAr detector was installed on surface at CERN and tested in 2010 and 2011 and it has been moved to its current location, the Underground Canfranc Laboratory (LSC), on February 2012.

In ArDM, the direct detection of WIMPS can be achieved by measuring the energy deposited when WIMPs elastically scatter from ordinary target argon nuclei. As we have mentioned before, the kinetic energy of these recoils is in the range of $\sim 1-100\,\text{keV}$ and the cross section is predicted to be weak-like [18].

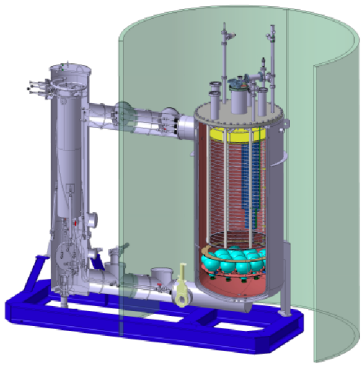

Figure 1: 3D model of the ArDM setup including the dewar, the cryo-system and the main measurement systems. The charge readout system is represented in yellow while the PMTs are shown in cyan and the green half cylinder indicates the outer dimension of the neutron shield.

When WIMPS go through the sensitive target, they produce nuclear recoils of the argon atoms as a consequence of their scattering. Then, the recoiling nuclei produce ionization and excitation of the atoms in liquid, that can form molecular bound states, called dimers[2], with other atoms in picoseconds time scale.

The excited diatomic molecules or excimers, such as $Ar_2{}^*$, are dimers with associated excited electronic states and dissociative ground states [19]. At the same time, argon ion results in the formation of excimers $Ar_2{}^*$ by recombination of Ar_2^+ with a free electron coming from the atomic argon ionization (Figure 2).

The $Ar_2{}^*$, which can exist in either singlet or triplet states with very different lifetimes, decays radiatively. The lowest allowed radiative decays from the molecular excited states are the transitions from the singlet and the triplet states ($^1\sum_u^+$ and $^3\sum_u^+$) to the ground state ($^1\sum_g^+$) which consist of two independent atoms. The emission spectrum for those transitions has a narrow peak at (128 ± 10) nm in the Vacuum Ultra Violet (VUV) band. This scintillation light (called primary scintillation, S1) cannot be reabsorbed by neutral argon atoms because the energy of the single atomic excited state is too high and it propagates in the detector. Only impurities such as N_2 and CO_2 can eventually reabsorb VUV light and capture the electrons.

[2] Dimers are chemical entities consisting of two structurally similar atoms or molecules joined by bonds that can be either strong or weak, covalent or intermolecular.

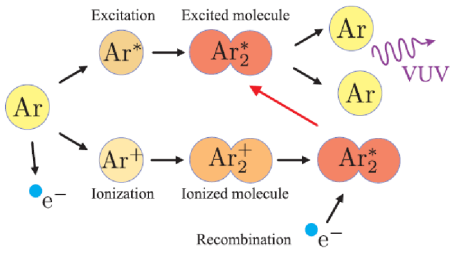

Figure 2: Diagram of ionization and excitation liquid argon processes.

The reflector surrounding the sensitive volume is coated with a wavelength shifter (tetraphenylbutadiene, TPB) to improve the light collection efficiency of the detector (see [20] for coating techniques). As soon as the primary photons reach the reflectors, they are converted and re-emitted with the optimal wavelength (≈ 420 nm) for its detection. The re-emitted light can reach the bottom or the top of the detector, where two arrays of 14 hemispherical Hamamatsu photomultipliers (PMT) are located. The surface of the PMTs is also coated with a wavelength shifter to detect the direct light, which is approximately 10% of the total light.

The electrons produced by the interaction in liquid that do not recombine with the parent ions are drifted towards the interface liquid-gas by a uniform electric field perpendicular to the readout plane (Figure 3). These electrons are extracted and accelerated from the liquid into the gas phase applying an electric field of 4 kV/cm, thus producing secondary scintillation light in gas (S2). The amount of light produced is directly proportional to the amount of charge reaching the gas phase, which is at the same time proportional to the amount of charge initially produced by the interaction.

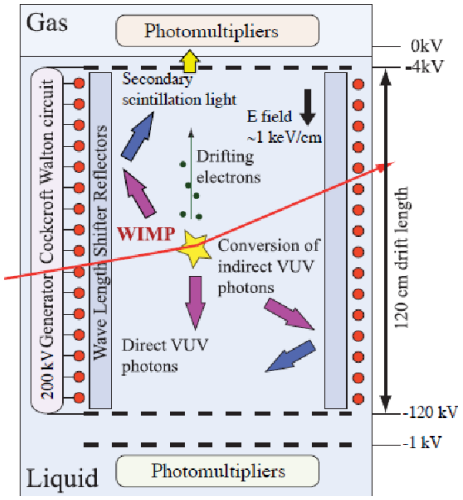

Figure 3: Conceptual design of the ArDM experiment.

Since the electron diffusion during the charge drift is low in noble liquids ($\approx$ mm), the xy position of the interaction is preserved and it can be measured through the light pattern of the PMT top array. Taking into account the drift time, measured as the delay of S2 respect to S1, the z coordinate can be also reconstructed, thus allowing to the ArDM time projection chamber (TPC) to provide the three-dimensional position information [21].

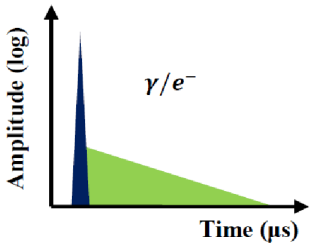

Figure 4: Scintillation topology of the $\gamma - e^-$-like process.

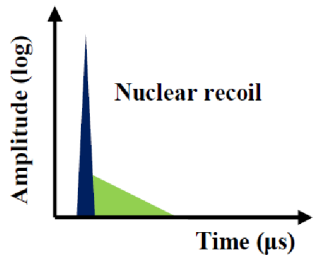

Figure 5: Scintillation topology of the nuclear recoil process.

The relative amount between the extracted and drifted electrons depends on the charge track structure besides the drift field. Consequently, the ratio between the two amplitudes of the scintillation signals, S1 and S2, is different for different interaction types and it can be used for discriminating the nuclear recoil from the electron interactions. Additionally, the two transitions ${}^1\sum_u^+ \rightarrow {}^1\sum_g^+$ and ${}^3\sum_u^+ \rightarrow {}^1\sum_g^+$ from excited dimers states to the ground state have different decay times, that will be called τ_s for the singlet and τ_t for the triplet. This is due to the fact that the first one is strongly allowed ($\tau_s \simeq 5\,\text{ns}$) while the second is allowed only because of the spin-orbit coupling ($\tau_t \simeq 1.6\,\mu\text{s}$). The ratio between the populations of the two initial states, $r = \delta({}^1\sum_u^+)/\delta({}^3\sum_u^+)$, depends on the ionization density of the track and, consequently, it is quite different for electron/photon interactions ($r \approx 1/2$) and nuclear recoil ($r \approx 4/5$) [22], thus giving an additional and independent background rejection tool. The corresponding typical signals are represented in Figures 4 and 5. In this context, the possibility to measure both ionization charge and time evolution of the associated primary scintillation light allows high nuclear recoil discrimination, rejecting the more abundant interactions given by photons and electrons[3].

While the gamma and electron interactions can be rejected, it is hard to distinguish neutrons from WIMPs because both do not have electromagnetic charge and produce nuclear recoils. However, they have different energy spectra and scatter multiplicities: we have calculated that at least 50% of neutrons scatter more than once and only 10% of the total number of neutrons produce a single recoil event in the energy range of interest.

IV. DETECTOR CALIBRATION

The appropriate detector calibration at low energies is essential in order to determine the energy threshold and WIMP sensitivitity, since the expected dark matter signal has energies of tens of keV and drops exponentially with the energy (equation (4)). For the ArDM experiment, both neutron and gamma calibration will be performed. The neutron calibration is important to asses the detector response to the nuclear recoil. In addition, periodic runs with low energy gamma sources are required in order to establish the energy scale, monitoring, at the same time, the stability of the detector's behavior. In the present work, we are going to focus on gamma calibration.

Due to the large size of the ArDM detector and its shielding capability against external radiation, reaching the central volume of the liquid with external gamma rays becomes difficult at low energies. All the calibrations should be performed in a sealed environment with the same experimental conditions as the physics runs. For these reasons, dedicated calibration systems should be designed to place the source between the detector and the external polyethylene shield.

A setup for periodic gamma calibration, referred to as *Calibration I*, has been specifically designed. It consists of a pair of pipes made of a plastic material. One of the pipes will run parallel to the dewar wall and the other will surround it (Figure 6), so calibration for different x, y, z positions will be possible. According to this setup, a commercial stainless steel encapsuled gamma source could be the most appropriate choice. It can be attached to a flexible rod and guided inside one of the pipes and, if this rod is graduated, it is immediate to know the source position.

[3] The most important contribution to the background is due to the ^{39}Ar isotope, whose activity is $\simeq$ 1Bq/kg of liquid [23].

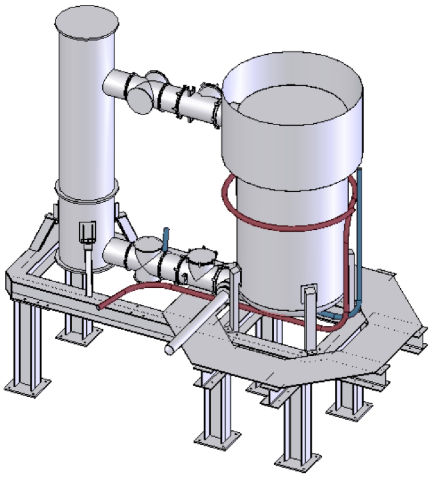

Figure 6: Detector layout with gamma calibration setup.

For the neutron calibration, a drawer is going to be made by cutting off a small block at a middle height of the polyethylene shield. This polyethylene block would be removed during the calibration procedures. This setup, named *Calibration II*, can also be used for gamma calibration with a collimated source. In this way, six lead bricks, one of them with a hole (10 mm radius and 204 mm length) drilled in the direction of the detector center, will be placed inside the drawer (Figure 7).

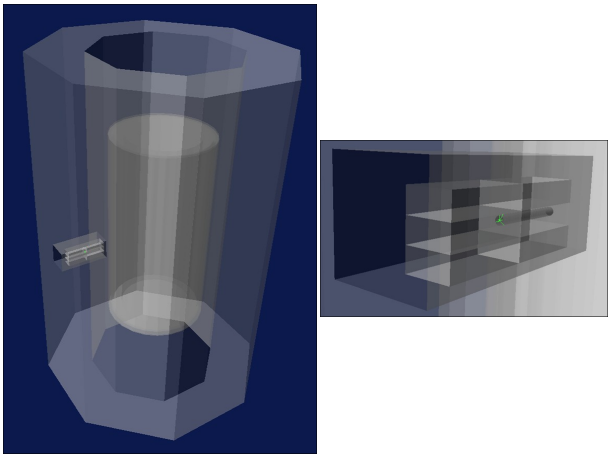

Figure 7: Setup for the neutron and collimated gamma calibration.

A preliminary study based on cross section and attenuation of a photon beam in liquid argon has been undertaken in order to constrain the most appropriate gamma energy in a certain range. The optimal energy should allow a substantial number of photons to go through the stainless steel walls of the dewar without being stopped and cross the borders of the active volume into the center of the detector. A significant number of photoelectric interactions would be necessary in order to clearly measure the energy released in the interaction location. However, we should take into account that the photoelectric cross section decreases with energy while the probability of a photon to reach the sensitive volume increases with energy. According to the previous considerations, the most suitable energy range for our purpose begins around 100 keV. Although ^{57}Co (85.6% E_γ=122 keV and 10.7% E_γ=136 keV) and ^{75}Se (58.3% $E_\gamma = 136$ keV and 58.9% $E_\gamma = 265$ keV) were suggested as possible candidates in the considered energy range, a detailed Monte Carlo simulation is required in order to investigate the type and activity of the gamma source needed to efficiently calibrate the Ar TPC.

V. MONTE CARLO SIMULATION

Some Monte Carlo simulations have been carried out to check the behavior of different gamma sources in the ArDM experiment. In order to simulate the passage of particles through matter, Geant4 software toolkit [24] and its electromagnetic physics list have been used. Additionally, our results have been obtained with GAMOS [25], a framework for fast and flexible Geant4 application developed at CIEMAT.

In our research for the best gamma source for calibration, we followed a strategy consisting of several steps. First, we simulated the experiment geometry. It has been important for the simulation to note that the ArDM dewar is made of several walls, the internal ones containing liquid argon and the most external bounding a vacuum region. These liquid argon layers provide thermal stability to the active volume inside, while the vacuum layer isolates the system from environmental temperature. All the dewar walls have been simulated with their actual thickness and made of the stainless steel predefined in the Geant4 material database.

Different simulations have been carried out modeling both Calibration I and II experimental setups described in the previous section. The modeling of the dewar is based on a simplified geometry, build up from cylinders in order to reproduce the dewar walls. The inner cylinder has a 500 mm radius, while the outer cylinder radius is 560 mm. The total height of the dewar is 2093 mm. We have also taken into account that the sensitive volume, represented by an internal cylinder of 400 mm radius, is limited by the wavelength shifter reflectors.

For the Calibration I setup modeling, a point like gamma source with isotropic emission has been placed at medium height and 40 mm distance from the outer dewar wall, which is approximately the distance where the vertical pipe is installed (Figure 8). This geometry is the one used for an energy scanning simulation, which is required to asses the most appropriate energy and activity of the gamma calibration source. The energy range con-

sidered for the scanning simulation goes from 100 keV up to 450 keV with steps of 50 keV, although smaller steps of 25 keV were considered for the most interesting energy range. In order to have enough statistics, $2e^6$ events were simulated for energies above 150 keV and $4e^6$ events for lower energies.

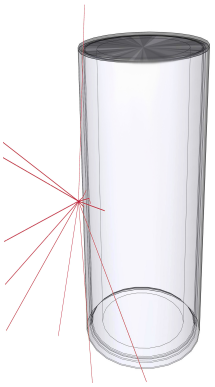

Figure 8: Dewar geometry used for energy scanning simulations. Some primary gamma tracks are depicted in red.

The analysis of the energy deposited in the active volume and the position of the photoelectric interaction have been considered for selecting the most appropriate gamma source for calibration. It has also been important to study the probability of interaction as well as the ratio between the total number of photoelectric and multiple interaction events for the different processes occurring within the detector sensitive volume. Figure 9 shows the energy deposited for two different simulations corresponding to 125 keV and 175 keV.

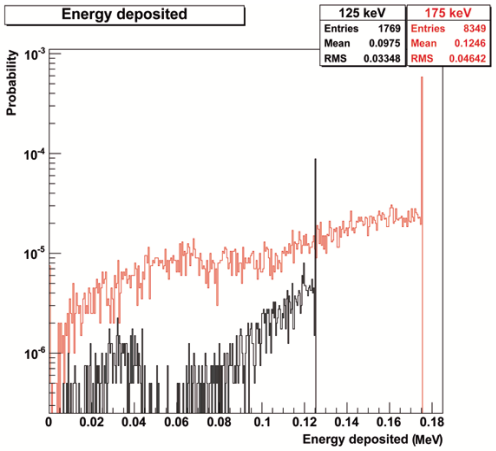

Figure 9: Energy deposited in the sensitive volume by 125 keV and 175 keV gamma sources for Calibration I setup.

The spectrum has a similar structure for both energies, consisting of the full energy peak, whose energy is equal to the one of the primary gamma, and a compton tail. Both multiple and single (photoelectric) interaction are included in the full energy peak. Comparing the spectra of 125 keV and 175 keV, we can point out some important differences. As expected, the probability of producing an interaction in the sensitive volume is lower for 125 keV than for 175 keV, since for higher energies there are more primary photons that can reach the detector's sensitive volume. Additionally the 175 keV spectrum shows a higher full energy deposition peak with a bigger probability of single interaction ($6.75 \cdot 10^{-5}$) than the 125 keV one ($2.25 \cdot 10^{-6}$). At the same time, the compton tail is much bigger for 175 keV than for 125 keV.

An important parameter for our simulation is given by the single photoelectric interaction in the full energy peak because it allows to calibrate the detector in terms of energy and interaction position. Additionally, given the good discrimination of multiple and single interactions of ArDM, the single events can be easily selected. In order to have a better comparison of the different simulations, the results for Calibration I have been summarized in table I.

E_i	PH prob	PH ev/h/100 kBq	Mult ev/h/100 kBq	Ratio
100	$(2.25 \pm 0.75) \cdot 10^{-6}$	$(8.1 \pm 2.7) \cdot 10^{2}$	$(7.92 \pm 0.84) \cdot 10^{3}$	$(1.02 \pm 0.36) \cdot 10^{-1}$
125	$(1.80 \pm 0.21) \cdot 10^{-5}$	$(6.48 \pm 0.76) \cdot 10^{3}$	$(1.526 \pm 0.037) \cdot 10^{5}$	$(4.25 \pm 0.51) \cdot 10^{-2}$
150	$(4.85 \pm 0.49) \cdot 10^{-5}$	$(1.75 \pm 0.17) \cdot 10^{4}$	$(6.32 \pm 0.11) \cdot 10^{5}$	$(2.76 \pm 0.28) \cdot 10^{-2}$
175	$(6.75 \pm 0.58) \cdot 10^{-5}$	$(2.43 \pm 0.21) \cdot 10^{4}$	$(1.476 \pm 0.016) \cdot 10^{6}$	$(1.65 \pm 0.14) \cdot 10^{-2}$
200	$(5.75 \pm 0.54) \cdot 10^{-5}$	$(2.07 \pm 0.19) \cdot 10^{4}$	$(2.509 \pm 0.021) \cdot 10^{6}$	$(8.25 \pm 0.77) \cdot 10^{-3}$
250	$(6.10 \pm 0.55) \cdot 10^{-5}$	$(2.20 \pm 0.20) \cdot 10^{4}$	$(4.844 \pm 0.030) \cdot 10^{6}$	$(4.53 \pm 0.41) \cdot 10^{-3}$
300	$(6.10 \pm 0.55) \cdot 10^{-5}$	$(2.20 \pm 0.20) \cdot 10^{4}$	$(7.261 \pm 0.036) \cdot 10^{6}$	$(3.02 \pm 0.27) \cdot 10^{-3}$
350	$(4.10 \pm 0.45) \cdot 10^{-5}$	$(1.48 \pm 0.16) \cdot 10^{4}$	$(9.435 \pm 0.041) \cdot 10^{6}$	$(1.56 \pm 0.17) \cdot 10^{-3}$
400	$(4.15 \pm 0.46) \cdot 10^{-5}$	$(1.49 \pm 0.16) \cdot 10^{4}$	$(1.1498 \pm 0.0046) \cdot 10^{7}$	$(1.30 \pm 0.14) \cdot 10^{-3}$
450	$(3.75 \pm 0.43) \cdot 10^{-5}$	$(1.35 \pm 0.16) \cdot 10^{4}$	$(1.3304 \pm 0.0049) \cdot 10^{7}$	$(1.01 \pm 0.12) \cdot 10^{-3}$

Table I: Results for the photoelectric probability of interaction in the full energy peak, photoelectric events per hour and per 100 kBq, multiple interaction events per hour and per 100 kBq and ratio between the total number of photoelectric and multiple interaction events corresponding to Calibration I setup for different energies, E_i.

The photoelectric probability in the full energy peak (column 2) increases with energy, it reaches a maximum for an energy around 175 keV and then decreases. This is given by the fact that photoelectric cross section decreases with energy, while the probability of a photon to reach the sensitive volume increases, as mentioned before.

Considering a source with an activity of 100 kBq, $\sim 6.5e^3$ photoelectric interactions per hour are expected for 125 keV and $\sim 2.4e^4$ for 175 keV. While the photoelectric probability increases and reaches a maximum, the number of multiple interaction only increases with energy.

The radial position of the photoelectric interaction shows how the events are distributed and their distance from the center of the detector. Figure 10 shows that the events for Calibration I (black line) are not distributed quite deep inside the detector. For this reason, Calibration II was suggested in order to try to have as many events located deeper as possible in the sensitive volume and also to improve, eventually, the ratio between photoelectric and multiple interaction events.

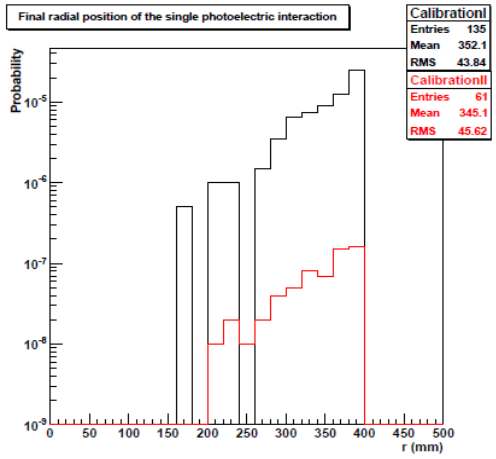

Figure 10: Radial position of the photoelectric interaction for a 175 keV gamma source. The results for Calibration I and II setups are displayed.

Calibration II corresponds to the collimated gamma calibration setup. Apart from the dewar, the geometry used for this simulation includes the polyethylene shield and the lead bricks setup for collimation shown in Figure 7. Since the photoelectric probability had a maximum at 175 keV in Calibration I, for Calibration II we have simulated energies in a narrow range that goes from 125 keV to 200 keV. Proceeding analogously as what we did for Calibration I, we have represented the energy deposition histogram, Figure 11. As in the previous case, the histogram shows a full energy deposition peak, and a compton tail, which are higher and longer respectively for 175 keV than for 125 keV.

The complete results from Calibration II simulation are summarized in table II, where the same quantities included in Table I are shown for Calibration II.

Relevant information can be extracted from the comparison of the energy histograms for both calibrations. On the one hand, for Calibration II there are less energy deposited events registered due to the fact that the solid angle of particle emission is much smaller. On the other hand, the less populated compton tail indicates that in this case the photoelectric/multiple interaction ratio has been improved. This fact can be checked by comparing the last column of tables I and II.

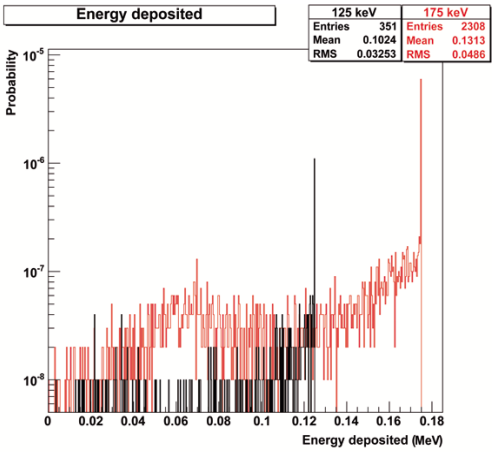

Figure 11: Energy deposited in the sensitive volume by 125 keV and 175 keV gamma sources for Calibration II setup.

E_i	PH prob	PH ev/h/100 kBq	Mult ev/h/100 kBq	Ratio
125	$(2.40 \pm 0.49) \cdot 10^{-7}$	$(8.6 \pm 1.8) \cdot 10^{1}$	$(1.177 \pm 0.065) \cdot 10^{3}$	$(7.3 \pm 1.6) \cdot 10^{-2}$
150	$(5.30 \pm 0.73) \cdot 10^{-7}$	$(1.91 \pm 0.26) \cdot 10^{2}$	$(4.06 \pm 0.12) \cdot 10^{3}$	$(4.70 \pm 0.66) \cdot 10^{-2}$
175	$(6.10 \pm 0.78) \cdot 10^{-7}$	$(2.20 \pm 0.28) \cdot 10^{2}$	$(8.09 \pm 0.17) \cdot 10^{3}$	$(2.72 \pm 0.35) \cdot 10^{-2}$
200	$(8.80 \pm 0.94) \cdot 10^{-7}$	$(3.17 \pm 0.34) \cdot 10^{2}$	$(1.294 \pm 0.022) \cdot 10^{4}$	$(2.45 \pm 0.26) \cdot 10^{-2}$

Table II: Results for the photoelectric probability of interaction in the full energy peak, photoelectric events per hour and per 100 kBq, multiple interaction events per hour and per 100 kBq and ratio between photoelectric and multiple interaction corresponding to Calibration II setup for different energies, E_i.

If we focus on the radial position of the photoelectric interaction (Figure 10 red line), the mean value is lower for Calibration II than for Calibration I, meaning that we achieved a slight improvement in the depth distribution of the photoelectric interactions. More simulations are currently being carried out with different collimator geometries.

While the results of the simulations suggest that the biggest probability of photoelectric in the full energy peak can be obtained around 175 keV, we give more importance to the photoelectric over compton ratio, which is maximum at 125 keV. As a result of the previous considerations, ^{57}Co (85.6% E_γ=122 keV and 10.7% E_γ=136 keV), whose half-life is 271.79 days, can be a possible source choice for our gamma calibration. For this rea-

son, Calibration I and Calibration II simulations have been carried out for a monoenergetic 122 keV line. The results, shown in Table III, confirm the better ratio obtained with the collimated source.

C	PH prob	PH ev/h/100 kBq	Mult evh/100 kBq	Ratio
I	$(1.80 \pm 0.30) \cdot 10^{-5}$	$(6.5 \pm 1.1) \cdot 10^{3}$	$(1.229 \pm 0.047) \cdot 10^{5}$	$(5.3 \pm 1.9) \cdot 10^{-2}$
II	$(1.90 \pm 0.44) \cdot 10^{-7}$	$(6.8 \pm 1.6) \cdot 10^{1}$	$(9.36 \pm 0.58) \cdot 10^{2}$	$(7.31 \pm 0.39) \cdot 10^{-2}$

Table III: Results for 122 keV photoelectric probability of interaction in the full energy peak, photoelectric events per hour and per 100 kBq, multiple interaction events per hour and per 100 kBq and ratio between photoelectric and multiple interaction corresponding to Calibration I and Calibration II setups.

In order to have realistic spectra it is crucial to take into account the energy resolution of the detector. We have based our analysis on the published results from XENON100 experiment [27] regarding the measured resolution (σ/E) for different gamma calibration lines. The energy dependence of the resolution is described by the following expression:

$$\frac{\sigma(E)}{E} = \frac{c_1}{\sqrt{E}} + c_2, \tag{6}$$

where E is the energy of the gamma, σ corresponds to the gaussian distribution that gives the energy resolution and c_1 and c_2 are constants. We have convoluted the energy deposited by 122 keV and 175 keV monoenergetic lines for both Calibration I and II with energy resolution, considering three different cases: energy resolution for XENON100 and two values worsened by 20% and 40%.

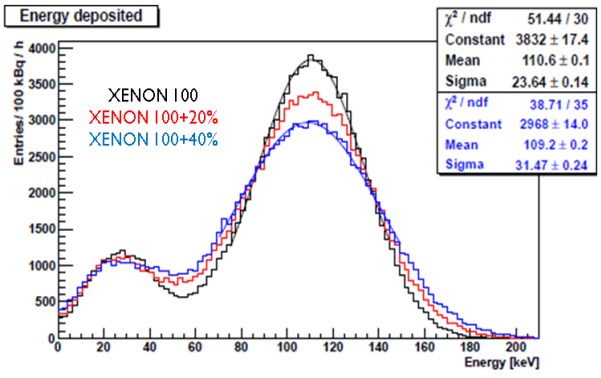

Figure 12: Energy deposited in the sensitive volume by a 122 keV gamma source for the Calibration I setup considering different energy resolutions.

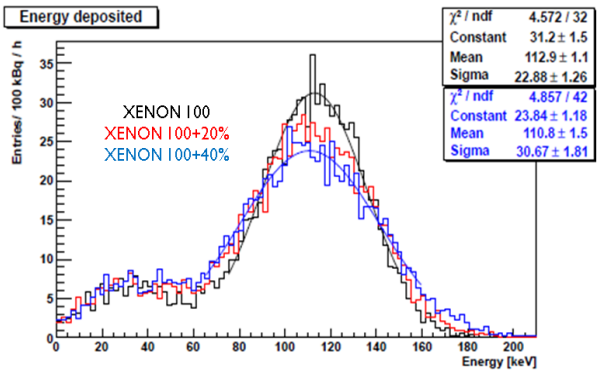

Figure 13: Energy deposited in the sensitive volume by a 122 keV gamma source for the Calibration II setup considering different energy resolutions.

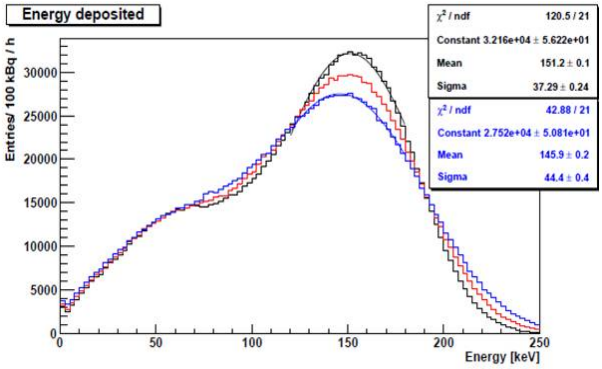

Figure 14: Energy deposited in the sensitive volume by a 175 keV gamma source for the Calibration I setup considering different energy resolutions.

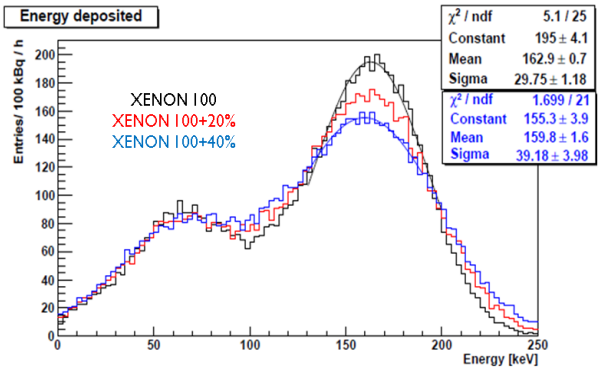

Figure 15: Energy deposited in the sensitive volume by a 175 keV gamma source for the Calibration II setup considering different energy resolutions.

Comparing the spectra obtained considering the three resolutions for 122 keV (Figures 12 and 13) and 175 keV

(Figures 14 and 15) photons with the two calibrations setups, the gaussian fit of the full energy peak has a mean value lower than the nominal energy because of the contribution of the compton tail. That systematic effect is bigger for worse resolutions and higher energies. At the same time the reduction of the compton tail in the collimated case can offer the best chance for a more precise energy calibration.

VI. CONCLUSIONS AND PROSPECTS

Monte Carlo simulations of the ArDM detector have been carried out in order to study gamma calibration of the detector. The deposited energy spectra and the single and multiple interaction rates have been considered to choose the optimal energy for the source. While the highest probability of single interaction in the full energy peak has been obtained for 175 keV, a better single/multiple ratio has been evidenced for 125 keV. Additionally, a more precise calibration in terms of energy and position can be obtained by collimating the beam with a proper setup. According to the previous considerations, a possible choice for gamma calibration is ^{57}Co (85.6% E_γ=122 keV and 10.7% E_γ=136 keV), that is commercially available and has lifetime, 271.79 days, long enough for our purposes.

New simulations regarding the optimization of the gamma calibration setups and validation of the results with real data are currently ongoing.

[1] E. Komatsu et al., ApJS 192:18 (2011).
[2] V. Sahni, Lect. Notes Phys. **653** (2004) 141 [astro-ph/0403324].
[3] M. A. Sánchez, PhD thesis, Granada University (Spain), July 2009.
[4] G. Jungman,M. Kamiankosky,K. Griest, Phys. Rep. 267 (1996),195.
[5] G. Bertone, D. Hooper and J. Silk, Phys. Rept. **405** (2005) 279, arXiv:hep-ph/0404175v2.Conference
[6] S. P. Martin, In *Kane, G.L. (ed.): Perspectives on supersymmetry II* 1-153, arXiv:hep-ph/9709356v6.
[7] P. J. Fox, R. Harnik, J. Kopp and Y. Tsai, Phys. Rev. D **85** (2012) 056011 [arXiv:1109.4398 [hep-ph]].
[8] C. Munoz, 2012, arXiv:1203.0678 [hep-ph].
[9] J. D. Lewin and P. F. Smith, Astropart. Phys. 6, 87-112 (1996).
[10] SLAC dark matter summer school 2007. $http://www-conf.slac.stanford.edu/ssi/2007/talks/akerib_080207.pdf$.
[11] M. C. Carmona, PhD thesis, Granada University (Spain), May 2009.
[12] R. Bernabei et al., 2000, Phys. Lett. B 480, 23.
[13] R. Bernabei et al., 2008, Eur. Phys. J.C56, 333-355.
[14] CE. Aalseth et al., Phys. Rev. Lett. **107** (2011) 141301 [arXiv:1106.0650 [astro-ph.CO]].
[15] G. Angloher et al., Eur. Phys. J. C **72** (2012) 1971 [arXiv:1109.0702 [astro-ph.CO]]..
[16] D. Gastler et al., 2012, arXiv:1004.0373v3 [physics.ins-det].
[17] A. Rubbia, J.Phys.Conf.Ser. 39 (2006) 129-132, arXiv:hep-ph/0510320v1.
[18] C. Amsler et al. (The ArDM collaboration), JINST 5:P11003, 2010, arXiv:1009.3641v2 [physics.ins-det].
[19] JB Birks, Rep. Prog. Phys. 1975, 38, 903-974, doi:10.1088/0034-4885/38/8/001.
[20] V.Boccone et al. (ArDM collaboration), JINST 4:P06001, 2009, arXiv:0904.0246v1 [physics.ins-det].
[21] M. I. Lopes, V. Chepel, American Scientific Publishers (2005), ISBN: 1-58883-058-6.
[22] V. Boccone, 2008, arXiv:0810.4490v1 [physics.ins-det].
[23] P. Benetti et al. (WARP Collaboration), Nucl. Instrum. Meth. A 574, (2007) 83, arXiv:astro-ph/0603131v2.
[24] http://geant4.cern.ch/Geant4 Collaboration, Nuclear Instruments and Methods in Physics Research Section A: Accelerators, Spectrometers, Detectors and Associated Equipment, Volume 506, Issue 3, 1 July 2003, Pages 250303.
[25] http://fismed.ciemat.es/GAMOS/gamos.php.
[26] Eckert and Ziegler Group, http://www.ezag.com.
[27] E. Aprile *et al.* [XENON100 Collaboration], Astropart. Phys. **35** (2012) 573 [arXiv:1107.2155 [astro-ph.IM]].